NUMERICAL INVESTIGATION OF IMPACT OF NON-SPHERICAL PARTICLES WITH SPIN AND MULTI-POINT CONTACT

Xindong Xu, Kuahai Yu, Shile Yao, Shihong Xin

Department of Engineering Mechanics, Henan University of Science and Technology, Luoyang, China
e-mail: yukuahai@163.com

Zhufeng Yue, Lei Li

School of Mechanics, Civil Engineering and Architecture, Northwestern Polytechnical University, Xi'an, China

This paper investigates the dynamic behavior of elastoplastic collision of several non-sphere particles through the spherical element combination method. The particles are cylinder, triangle and square particles, which are combined by 2, 3 and 4 spheres using the spherical element method, respectively. Results reveal that the collision of the evaluated irregular particles exhibits three contact styles, which are single point contact, instantaneous multi-point contact and sequential multi-point contact. Normal contact torque and frictional torque act together on the spin of a particle and causes sequential multi-point contact under certain conditions for square particles.

Keywords: non-spherical particles, sphere element combination method, multi-point contact, coefficient of restitution, collision duration

1. Introduction

Many research fields involve collision and transport of diverse particles such as dust proof industrial equipment, desert formation and migration and treatment of atmospheric pollutants, etc. Natural particles are usually irregular, and it is difficult to describe their morphology. Thus, they are usually idealized to be spheres to simplify the simulation of particles transport, deposition and erosion, which also correspondingly results in simulation errors. In a sense, prediction of non-spherical particle collision characteristics has practical significance for development of particle flows and two-phase flows.

Most of the particle impact models are established with spherical assumption and elastic or elastoplastic theories. For example, Jackson and Green (2005) developed a spring damping model based on elastic contact theory by simplifying the particle-particle contact to a spring damping system, which was only available for the low velocity collision. Tabor (1951) divided the collision process into three stages: elastic compression, plastic compression and elastic rebound, and predicted the energy loss of each stage to calculate the coefficient of recovery (COR) of particle collision. Thornton (1997) proposed an elastic-plastic particle impact model. Furthermore, He and Wu (2008) developed an elastoplastic particle impact model based on the elastoplastic contact theory and the assumption of the elastoplastic strengthening criterion. Yu and Tafti (2016) proposed a novel collision model based on the Stronge model by incorporating a new recovery law. It could accurately predict the collision behavior of millimeter and micron sized particles. Then, they established the particle oblique impact model considering sliding and rolling (Yu *et al.*,2017) and developed an elastoplastic impact model considering the surface adhesion losses (Yu and Tafti, 2019).

However, theoretical method is difficult to describe details of particles deformation and contact forces during collision. In contrast, numerical simulation can sufficiently integrate the factors

of the particle geometry and well describe dynamic behavior of particle impact. In other words, numerical simulation is sensitive to reflect the particles morphology, material properties and impact velocity, etc. for particles collision. Wu *et al.* (2003) fitted a function of the coefficient of restitution varying with impact velocity and impact angle for spherical particles by numerical simulation. Kildashti *et al.* (2018) investigated the relationship of contact forces and the amount of overlapped ellipsoidal particles by the finite element method. Zhang and Vu-Quoc (2002) predicted collision characteristics between a sphere and a frictionless rigid surface by using the finite element method.

Unfortunately, most natural particles have random irregular shapes, and it is difficult to develop a unified model to predict particle impact behavior because of the diversity of particle geometry. A few studies investigate collision mechanisms of non-spherical particles and majority of them focus on certain specific geometries such as ellipsoidal, rectangular particles, etc. Gui *et al.* (2016) proposed an extended theoretical particle-wall collision model for rigid particles. It was validated by numerical simulation of the rectangular particle impact. Wynn (2009) investigated collision of ellipsoidal particles impact with a semi-infinite plane wall, and concluded that COR varies considerably with initial orientation and can be greater than unity. Furthermore, many irregular particle geometry modeling methods have been proposed recently, such as the hyper-quadric surface method (Cui *et al.*, 2013; Wang and Ji, 2018) and the spherical element combination method (Favier *et al.*, 1999; You and Zhao, 2018), etc. Höhner *et al.* (2011) completed simulation of irregular particles impact on a flat wall using the polyhedral geometry modeling method and the results showed that there was a non-negligible effect of shape approximation on the temporal force evolution in the normal and tangential direction. Kruggel-Emden *et al.* (2008) established a rigid composite particle by the multi-sphere method and concluded that the multi-point contact state of irregular particles and its collision dynamics remained to be further improved. Azimian *et al.* (2015) investigated the erosion mechanism of irregular particle impact to ductile copper target with spin. Kodam *et al.* (2009) predicted variation of contact forces between column particles and a wall.

This paper presents an investigation of several non-spherical particles collisions considering impact velocity, impact angle, particle spin and multi-point contact. The numerical model is verified by experimental data of spherical particles collision. The results can provide support for theoretical modeling of irregular particle collision, simulation of particle flow and multi-phase flow.

2.   Geometric model and collision prediction

A group of non-spherical particle geometries is constructed using the combined with spherical element method. The group includes double-sphere element cylinder particles, three-sphere elemental triangle particles and four-sphere element square particles. The discussed irregular particles are composed of the same sized 2, 3 and 4 spherical elements, respectively. The schematic diagram of particles combination and particle-wall collision are shown in Fig. 1. The central distance between adjacent elements is the same as the element radius. V_i and V_r are the impact velocity and rebound velocity, respectively. α is the impact angle and β is the rebound angle, γ is the angle between the impact velocity and particle axis I direction (dash dot line in the figure), and φ is the particle posture angle that is the angle between the axis I and the surface tangential direction. ω_i and ω_r are the impact angular velocity and the rebound angular velocity, respectively. It is assumed that the angular velocity counterclockwise direction is positive and the clockwise one is negative.

The total COR is the ratio of the particle recovery velocity and impact velocity $e = V_r/V_i$. The normal COR is the ratio of the rebound normal velocity and impact normal velocity, and there is $e_n = V_{nr}/V_{ni} = (V_r \sin\alpha)/(V_i \sin\alpha)$.
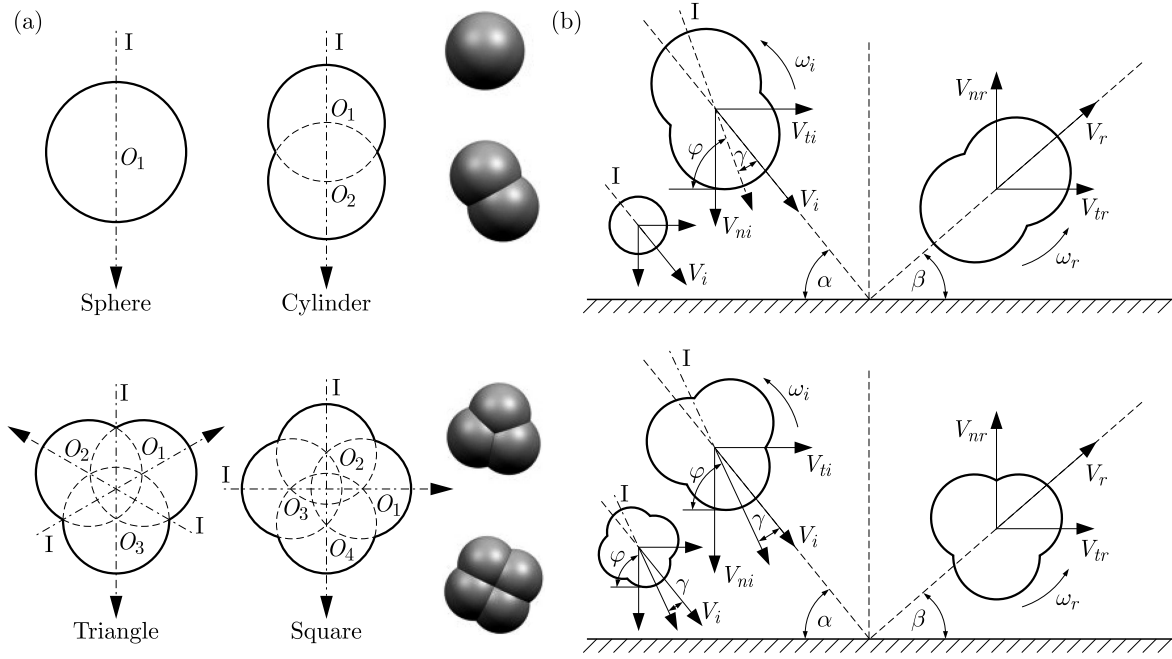
Fig. 1. Schematic diagram of the geometrical model and particle-wall collision

The duration of compression and rebound stages are the same for particle elastic collision, and can be calculated as follows (Deresiewicz, 1968)

$$t_e = 1.435 \sqrt[5]{\frac{m_*^2}{R_* E_*^2 V_{ni}}} \qquad (2.1)$$

Furthermore, the duration of compression and rebound stages for elastoplastic collision is suggested to be as follows (Ning, 1995):
— compression stage

$$t_c = \pi R_* \sqrt{\frac{\rho}{3\sigma_Y}} \qquad (2.2)$$

— rebound stage

$$t_r = \pi R_* \sqrt{\frac{5}{4}} e_n \sqrt{\frac{\rho}{3\sigma_Y}} \qquad (2.3)$$

where σ_Y, ρ and e_n are the yield stress of the particle, particle density and normal coefficient of restitution, respectively.

The average error η evaluates the accuracy of the numerical result, and it is

$$\eta = \sum_{i=1}^{n} \frac{1}{n} \Big(\frac{|\xi_{ei} - \xi_{pi}|}{\xi_{ei}} \cdot 100\% \Big) \qquad (2.4)$$

where ξ_{ei} is the experimental result, ξ_{pi} is the numerical result.

3. Collision simulation and verification

Two particle collision cases are employed to validate the particle elastoplastic collision model compared with experimental data. The first is a normal impact of 1.29 mm diameter steel particles with a steel wall (Kim and Dunn, 2007) and the second is a 0.1 mm diameter glass particles

impact with a steel wall at different impact angles (Sommerfeld and Huber, 1999). Table 1 shows material properties of the particles and walls. Figure 2 shows the geometry and mesh of particle collision of Case 1. A half of the model is used to reduce the computational cost, as the geometry and the load are symmetric with the plane $z = 0$. Mesh generation uses hexahedral elements with a minimum size of $0.1\,\mu$m and refines the grid at the contact region to improve the accuracy. The total mesh of the sphere and wall are about 80 000 and 160 000, respectively. Mesh independence is verified.

Table 1. Particle and wall material properties

Case	Object	Material	Density [kg/m³]	Young's modulus [GPa]	Poisson's ratio	Yield stress [MPa]	Diameter [mm]
1	Particle	Steel	7850	210	0.30	1410	1.29
	Wall	Steel	7850	205	0.30	345	–
2	Particle	Glass	2200	72	0.17	1100	0.1
	Wall	Steel	7850	210	0.30	205	–

The bottom surface ($y = 0$) is fixed and the top surface is free. A symmetry condition is applied at the symmetry plane ($z = 0$) and non-reflecting boundary conditions are applied to the lateral faces of the target wall. The bilinear isotropic constitutive model describes the stress-strain response of materials for deformations of the particle and wall and covers the range from elastic to plastic one. Contact detection between the particle and wall uses a surface-to--surface automatic contact algorithm. The static and dynamic friction coefficients of Case 1 are 0.3 and 0.1, respectively. Table 2 shows the static and dynamic friction coefficients varying with the impact angle of Case 2 (Abedi, 2009).

Table 2. Friction coefficient between the particles and wall

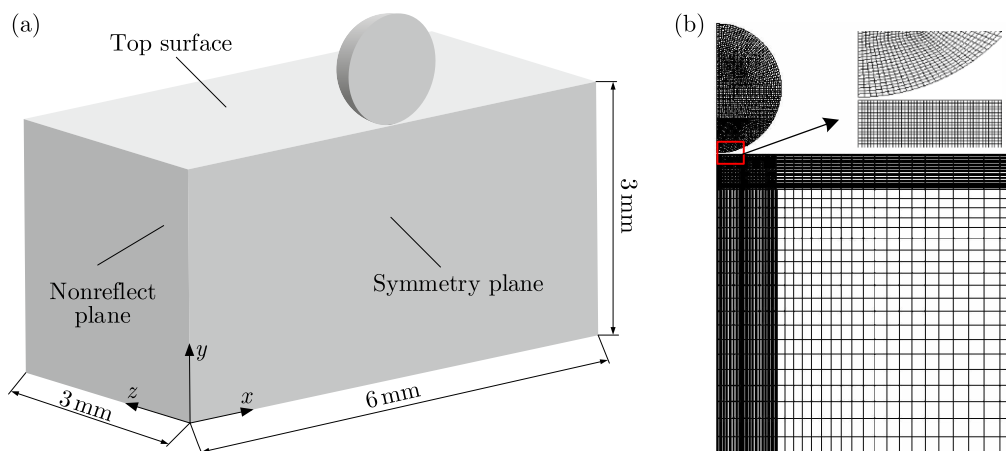| α [°]	2	7	12	17	22	27	32	37	42
μ	0.375	0.375	0.20	0.18	0.10	0.10	0.10	0.09	0.09

Fig. 2. Geometry of the model and the mesh of test Case 1

Figure 3 shows differences between the current numerical results with the experimental ones (Kim and Dunn, 2007; Sommerfeld and Huber, 1999) and the numerical result of Abedi (2009). Both the current result and Abedi's result are well fit to the experimental data. The average errors of the current result are 4.5% and 2.8%, respectively. Abedi's result gives 14.25% and 3.2%, respectively. It shows that the present model can well predict the particle collision behavior.
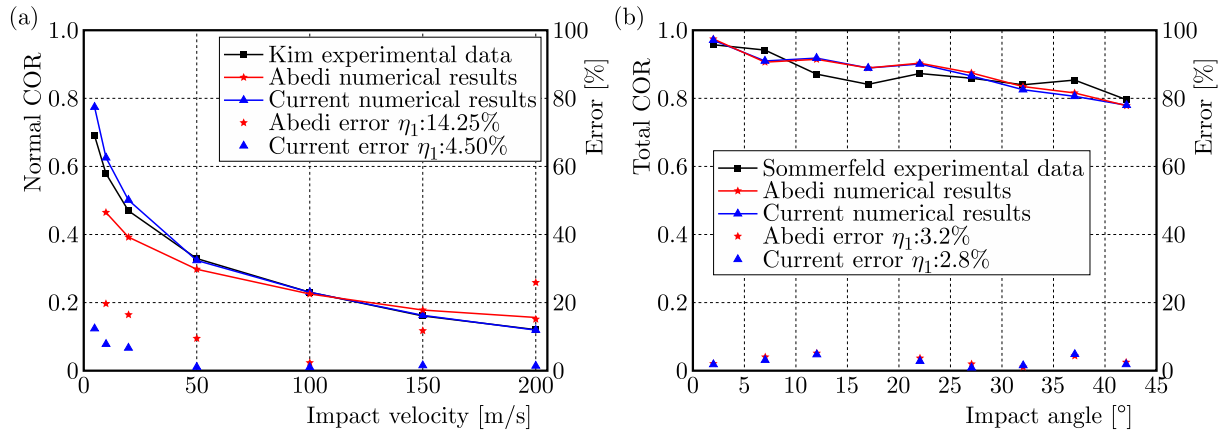

Fig. 3. Comparison of numerical and experimental results: (a) Case 1, (b) Case 2

Figure 4 shows the normal contact force varying with the impact process for impact velocities of 10 m/s and 50 m/s of Case 1. The normal contact force keeps the zero value at the beginning, i.e. for the initial gap between the particle and wall, and gets larger after the contact between the particle and wall starting. The contact force keeps on rising in the compression process until the maximum value is reached when the particle velocity is zero. Then the contact force falls during the rebound process and becomes zero at the end of the collision. Elastic potential energy converts to particle kinetic energy in the rebound stage. Collision duration is equal to the sum of compression and rebound stage duration. The predicted collision duration of the 1.29 mm particle impact at 10 m/s and 50 m/s is 4.1 μs and 3.1 μs, corresponding to the theoretical result of 3.9 μs and 3.5 μs obtained by Eqs. (2.2) and (2.3). The difference between the numerical and theoretical results are 5.1% and 11.5%, respectively.
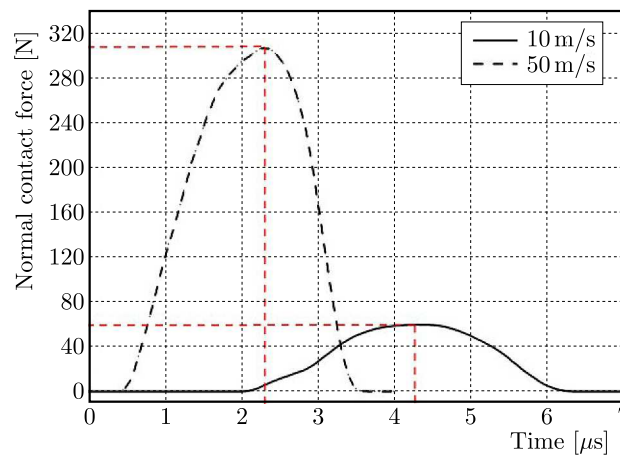

Fig. 4. Normal contact forces varying with the particle impact time in Case 1

4.   Non-spherical particles collision

This Section presents numerical investigations of the three discussed non-spherical particle impacts at different velocities and postures, with the equivalent diameter of 1.29 mm. The spherical element diameters of the double-sphere element cylinder particle, three-sphere element triangle particle and the four-sphere element square particle are 1.084 mm, 0.988 mm, and 0.916 mm, respectively. The meshing of the non-spherical particles and the wall in the finite element model is shown in Fig. 5. The current wall size, material model and the boundary conditions are the same as in Case 1 in Section 3. Multi-point contact will happen for the irregular particle impact with a flat surface, and makes the collision more complicated than in the spherical particles collision. Figure 6 shows a schematic diagram of multi-point contact for the evaluated particle impact with a flat surface, which is instantaneous multi-point and sequential multi-point contact. The instantaneous multi-point contact means contact with the surface by two or more points at a moment, and the sequential multi-point contact means that the particle contacts with the surface more than one time in a short period.
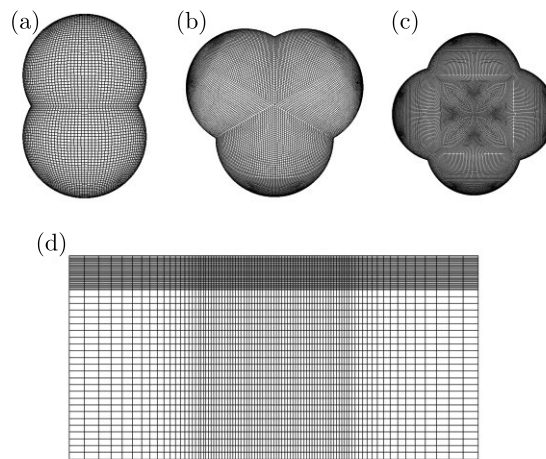

Fig. 5. Schematic diagram of meshing of non-spherical particles and wall: (a) cylinder, (b) triangle, (c) square, (d) wall
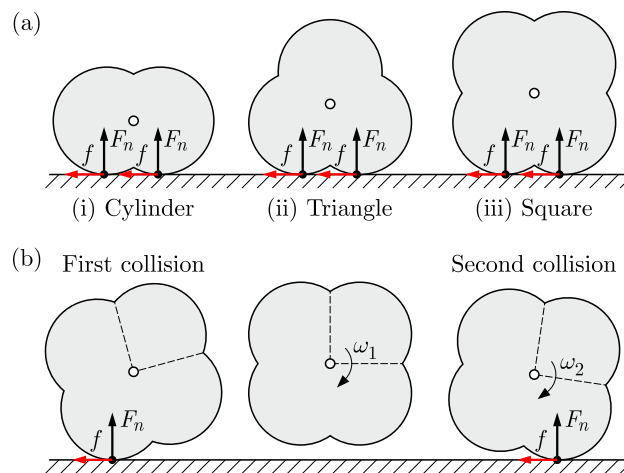

Fig. 6. Schematic diagram of multi-point contact of non-spherical particles: (a) instantaneous multi-point contact, (b) sequential multi-point contact

4.1. Normal collision

The normal impact (shown as in Fig. 1 of $\alpha = 90°$) means that the particle impact goes along the surface normal direction, otherwise an oblique impact happens. The orientation of the particle axis I decides about the particle impact posture. An instantaneous two-point contact happens for a double-sphere elemental cylinder particle normal impact when the axis I is parallel to the tangential surface, and the same condition happens while the posture angles φ (angle of direction of the axis I and the tangential surface) are $60°$ and $45°$ for the three-sphere element triangle particle and four-sphere elemental square particle, respectively.

Figure 7 shows the normal COR and collision duration of the three discussed particles of the normal impact at different velocities and postures. The normal COR decreases with the increasing impact velocity, and COR of instantaneous multi-point contact is usually higher than that of single point contact for a specified particle. The instantaneous multi-point contact has more elastic potential energy during the compression stage than the single-point contact and makes fewer plastic deformation losses. Collision duration decreases with the impact velocity, and varies between $2.5\,\mu s$ and $6.0\,\mu s$ for the discussed particles when the impact velocity is kept between $5\,m/s$ and $50\,m/s$. The duration of instantaneous multi-point contact is shorter than single-point contact for the same particle. It also shows significant differences for the normal COR and collision duration among the three discussed particles though they have the equivalent volume, impact velocities and impact postures. It indicates that the particle morphology and contact state have an effect on the particle collision behavior.
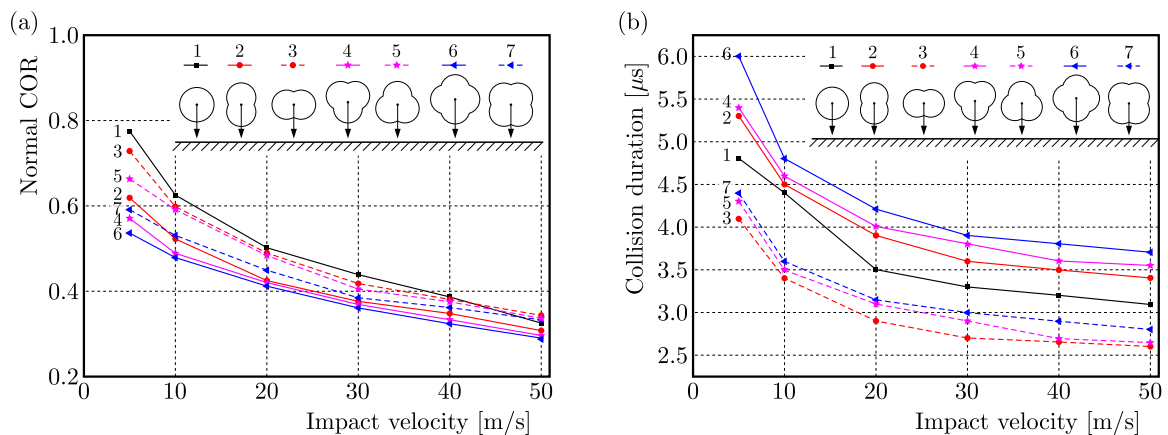

Fig. 7. Normal COR and collision duration of the particle impact in the normal without spin

4.2. Oblique collision

This Section presents the numerical prediction of the three discussed non-spherical particle oblique impacts at different velocities and angles. The direction of the normal contact force is considered to go through the center of mass for spherical particle collision. In that case, only the tangential force generates a rotational moment. In contrast, the direction of the normal contact force goes through the center of the contacted sphere element for the investigated three non--spherical particles. Both the normal and tangential forces create the particle spin. Therefore, it will generate a significant difference in collision characteristics between non-spherical and spherical particles of the oblique impact. And here, only the case in which the particle axis I is the same as the direction of impact velocity is investigated. In other words, the particle posture angle φ is equal to the impact angle α. The initial angular velocity of the particle is zero.

Figure 8 shows the normal COR curves of the three discussed particle oblique impacts with different angles and the impact velocities of $10\,m/s$ and $50\,m/s$. The normal COR decreases with the impact velocity of a specified particle with the same impact posture. However, there

are three contact types for the discussed non-spherical particles, which are single point contact, instantaneous multi-point contact and sequential multi-point contact. The impact angle (impact gesture) causes variation of the contact type, and leads to normal COR variation. There is only single point contact for the cylinder particle oblique impact. The maximum COR appears at the impact angles of 30° and 45° for the triangle and square particles when instantaneous multi-point contact happens. Interestingly, sequential multi-point contact happens for the square particle collision when the impact angle is 30° and the impact velocity is 50 m/s. In this case, the particle contacts with the target surface twice within a short time, and the normal COR rises from 0.12 to 0.37 for the first and second contact. Besides, the directions of normal contact forces torque of the first and second contact are opposite (shown in Fig. 6b), and this reduces the particle spin speed (shown in Fig. 9c). This means that a part of particle rotational kinetic energy transfers into normal translational kinetic energy during the second contact. Therefore, the particle spin causes continuous multiple collisions during the collision process in certain conditions, and affects particle collision dynamics, which is different from the single point contact of particle collision. This also illustrates that the impact angle and particle morphology have an effect on the normal COR.
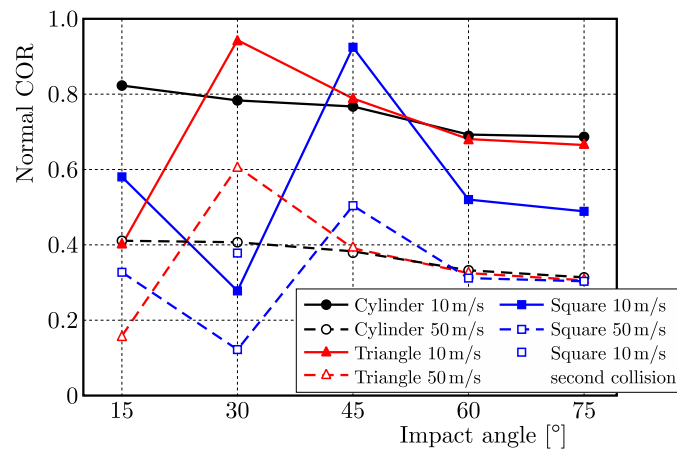

Fig. 8. Normal COR curves of non-spherical particles varying with the impact velocity

Figure 9 shows the rebound angular velocity of the three discussed particle oblique impacts with different velocities and impact angles. The present study investigates particles colliding with the impact angles of 15°, 30°, 45°, 60° and 75°. Not only the tangential force generates a particle spin torque, but also the normal contact force generates a non-spherical particles spin because of the contact point offset from the particle center. The magnitude of rebound angular velocity increases with the impact velocity for a specified impact angle. The cylinder particle spins counter-clockwise when the impact angles are 15° and 30°, whereas clockwise for the impact angles greater than 45°. The other particles spin counter-clockwise at evaluated impact angles, and the maximum rebound angular velocity appears at the impact angles of 15° and 30° for triangle and square particles, respectively, and the minimum rebound angular velocity appears at the impact angles of 45° and 75°. The particle spin obviously speeds up when the normal contact force torque is in the same direction as the tangential force torque. In contrast, the particles spin will be reduced. Furthermore, instantaneous multi-point contact happens at impact angles of 30° and 45° for the triangle and square particles. The direction of the normal contact force between the particle and wall at the two contact points is the same. Combined with the analysis in Fig. 7, the normal COR is larger than that of other single-point contacts, which is beneficial to an increase in the normal translation velocity. However, the two normal contact forces take moments on the centroid of the mass of the particles, and the two

moments are in opposite directions, which is not conducive to increasing the particle spin speed. Briefly, before and after the particle collision, the variation of angular velocity results from the combination of normal and tangential forces and makes the rebound angular velocity difficult to predict exactly.
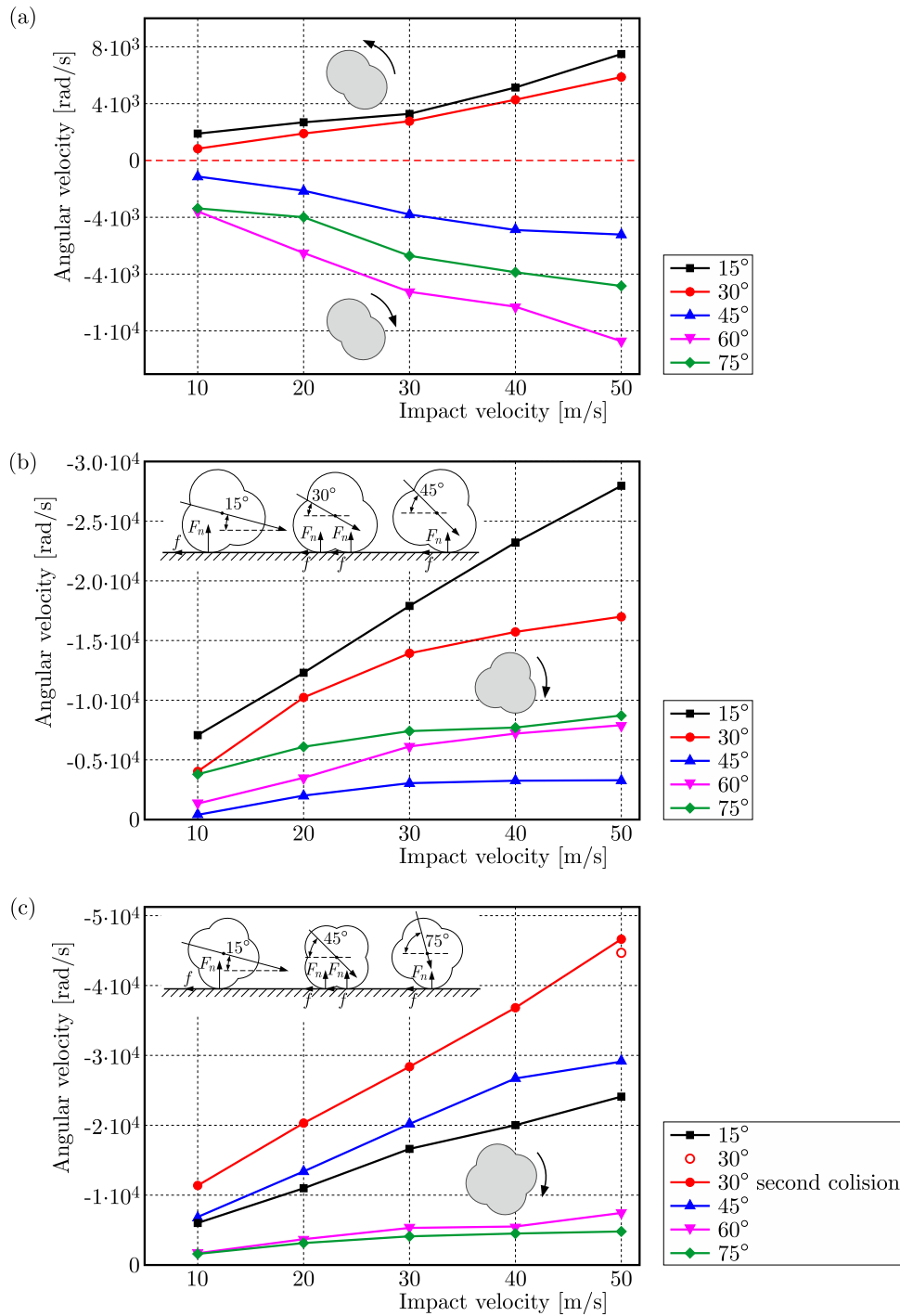

Fig. 9. Rebound angular velocity varying with the impact velocity for non-spherical particles: (a) cylinder particle, (b) triangle particle, (c) square particle

5. Conclusions

This paper investigates the impact dynamics of certain non-spherical particles. The spherical element combination method establishes geometry of a double-sphere element cylinder particle, three-sphere elemental triangle particle and four-sphere element square particle. The finite element method predicts the normal COR and rebounds the angular velocity for the particle impact with different velocities and angles. The main conclusions can be drawn as follows:

- The established FEM model can well predict rebound characteristics of the particle normal and oblique impact, validated by experimental data.
- Collision of non-spherical particles shows a more complicated contact process than that of spherical particles. There are three contact types of single-point contact, instantaneous multi-point contact and sequential multi-point contact during collision of the discussed three non-spherical particles.
- Normal COR and collision duration usually decrease with the impact velocity. Instantaneous multi-point contact and sequential multi-point contact happen under certain conditions for non-spherical particles. Contact details of non-spherical particles have a significant effect on collisions, which is different from single-point contact of the spherical particle collision.

References

1. ABEDI M., 2009, *Effect of Restitution Coefficient on Inertial Particle Separator's Efficiency*, Master's thesis, Northeastern University, Boston, Massachusetts

2. AZIMIAN M., SCHMITT P., BART H.J., 2015, Numerical investigation of single and multi impacts of angular particles on ductile surfaces, *Wear*, **342**, 252-261

3. CUI Z.Q., CHEN Y.C., ZHAO Y.Z., HUA Z.L., LIU X., ZHOU C.L., 2013, Study of discrete element model for non-sphere particles base on super-quadrics, *Chinese Journal of Computational Mechanics*, **30**, 854-859

4. DERESIEWICZ H., 1968, A note on Hertz's theory of impact, *Acta Mechanica*, **6**, 110-112

5. FAVIER J.F., ABBASPOUR-FARD M.H., KREMMER M., RAJI A.O., 1999, Shape representation of axi-symmetrical, non-spherical particles in discrete element simulation using multi-element model particles, *Engineering Computations*, **16**, 467-480

6. GUI N., YANG X.T., TU J.Y., JIANG S.Y., 2016, A generalized particle-to-wall collision model for non-spherical rigid particles, *Advanced Powder Technology*, **27**, 154-163

7. HE S.M., WU Y., 2008, Theoretical model on elastic-plastic granule impact, *Engineering Mechanics*, **25**, 12, 19-24

8. HÖHNER D., WIRTZ S., KRUGGEL-EMDEN H., SCHERER V., 2011, Comparison of the multi-sphere and polyhedral approach to simulate non-spherical particles within the discrete element method: influence on temporal force evolution for multiple contacts, *Powder Technology*, **208**, 643-656

9. JACKSON R.L., GREEN I., 2005, A finite element study of elasto-plastic hemispherical contact against a rigid flat, *Journal of Tribology*, **127**, 2, 343-354

10. Kildashti K., Dong K.J., Samali B.J., Zheng Q., Yu A., 2018, Evaluation of contact force models for discrete modelling of ellipsoidal particles, *Chemical Engineering Science*, **177**, 1-18

11. Kim O.V., Dunn P.F., 2007, A microsphere-surface impact model for implementation in computational fluid dynamics, *Journal of Aerosol Science*, **38**, 532-549

12. Kodam M., Bharadwaj R., Curtis J., Hancock B., Wassgren C., 2009, Force model considerations for glued-sphere discrete element method simulations, *Chemical Engineering Science*, **64**, 3466-3475

13. Kruggel-Emden H., Rickelt S., Wirtz S., Scherer V., 2008, A study on the validity of the multi-sphere discrete element method, *Powder Technology*, **188**, 153-165

14. Ning Z.M., 1995, *Elasto-Plastic Impact of Fine Particles and Fragmentation of Small Agglomerates*, The University of Aston in Birmingham

15. Sommerfeld M., Huber N., 1999, Experimental analysis and modelling of particle-wall collisions, *International Journal of Multiphase Flow*, **25**, 1457-1489

16. Tabor D., 1951, *The Hardness of Metals*, Clarendon Press, Oxford

17. Thornton C., 1997, Coefficient of restitution for collinear collisions of elastic-perfectly plastic spheres, *Journal of Applied Mechanics*, **64**, 383-386

18. Wang S.Q., Ji S.Y., 2018, Discrete element analysis of buffering capacity of non-spherical granular materials based on upper-quadric method, *Acta Physica Sinica*, **67**, 182-193

19. Wu C.Y., Thornton C., Li L.Y., 2003, Coefficients of restitution for elastoplastic oblique impacts, *Advanced Powder Technology*, **14**, 435-448

20. Wynn E.J.W., 2009, Simulations of rebound of an elastic ellipsoid colliding with a plane, *Powder Technology*, **196**, 62-73

21. You Y., Zhao Y.Z., 2018, Discrete element modelling of ellipsoidal particles using super-ellipsoids and multi-spheres: a comparative study, *Powder Technology*, **331**, 179-191

22. Yu K.H., Tafti D., 2016, Impact model for micrometer-sized sand particles, *Powder Technology*, **294**, 11-21

23. Yu K.H., Elghannay H., Tafti D., 2017, An impulse based model for spherical particle collisions with sliding and rolling, *Powder Technology*, **319**, 102-116

24. Yu K.H., Tafti D., 2019, Size and temperature dependent collision and deposition model for micron-sized sand particles, *Journal of Turbomachinery*, **141**, 1-11

25. Zhang X., Vu-Quoc L., 2002, Modeling the dependence of the coefficient of restitution on the impact velocity in elasto-plastic collisions, *International Journal of Impact Engineering*, **27**, 317-341